# Theoretical Study on Electronic and Spin Structures of $[Fe_2S_2]^{2+,+}$ Cluster: Reference Interaction Site Model Self-Consistent Field (RISM-SCF) and Multireference Second-Order Møller−Plesset Perturbation Theory (MRMP) Approach

**Masahiro Higashi and Shigeki Kato***

*Department of Chemistry, Graduate School of Science, Kyoto Unicersity, Kitashirakawa, Sakyo-ku, Kyoto 606-8502, Japan*

*Received: April 27, 2005; In Final Form: August 10, 2005*

Electronic structures of $[Fe_2S_2(SCH_3)_4]^{2-,3-}$ in DMSO solution are calculated using reference interaction site model complete active space self-consistent field (RISM-CASSCF)/multireference second-order Møller−Plesset perturbation theory (MRMP) method. For the reduced state, we obtain both the low-spin $Fe^{3+}Fe^{2+}$ localized and high-spin $Fe^{2.5+}Fe^{2.5+}$ delocalized forms, which are very close in energy. The spin interaction constants obtained from the energies of states with various spin multiplicities are in good agreement with the available experimental estimates both for the oxidized and for the reduced states. The dynamic electron correlation effect is found to be important in estimating the spin interaction between the Fe ions. The redox potentials are calculated to be 2.87 and 2.78 eV for the localized and delocalized reduced states, respectively, which are close to the experimental values. We devise a simple model for calculating the free energy curves of the reduction process based on the RISM-SCF theory. The activation barrier height is calculated to be 7.4 kcal/mol at the equilibrium geometry of oxidized state, indicating that the reduction reaction will occur efficiently in DMSO solvent. The effect of solvent fluctuation on the free energy profiles is discussed on the basis of the present calculations.

## 1. Introduction

Iron−sulfur proteins containing $Fe_2S_2$ clusters are known as major electron carriers in biological electron-transfer systems such as mitochondrial and photosynthetic chains.[1,2] Since their biological functions rely on the redox properties of the $Fe_2S_2$ core and their modulation by protein and solvent environments, many experimental[1−5] and theoretical[6−10] studies have been carried out to explore these issues for $Fe_2S_2$ ferredoxins and their synthetic analogues.

$Fe_2S_2$ clusters have reversible oxidized−reduced states as

$$[Fe_2S^*_2(SR)_4]^{2-} \rightleftharpoons [Fe_2S^*_2(SR)_4]^{3-} \qquad (1)$$

where S* denotes an inorganic sulfur bridging two Fe atoms and R is cysteine in proteins or, for example, an *o*-xylyl or phenyl group in their synthetic analogues. Although the ground state of the oxidized species has the singlet spin electronic structure where the two $Fe^{3+}$ ions with the spin quantum number $S = {}^5/_2$ are coupled antiferromagnetically,[5,11,12] that of the reduced form is still controversial. The low-spin $Fe^{3+}Fe^{2+}$ mixed valence electronic structure is generally considered to be the ground state where the $Fe^{3+}$ ($S = {}^5/_2$) and $Fe^{2+}$ ($S = 2$) ions are coupled through the antiferromagnetic exchange interaction, referred to as a localized state.[12] However, the high-spin valence delocalized state has been experimentally observed for Cys60Ser[13] and Cys56Ser[14] mutants of *Clostridium pasteurianum*, indicating that these proteins exist as mixtures of the $S = {}^1/_2$ localized and $S = {}^9/_2$ delocalized forms. Moreover, the delocalized high-spin $Fe^{2.5+}Fe^{2.5+}$ pairs are detected in the subunits of $[Fe_3S_4]^0$ and $[Fe_4S_4]^{3+,2+,+}$ iron−suflur proteins.[2] For example, two equivalent high-spin $Fe^{2.5+}Fe^{2.5+}$ pairs are antiferromagnetically coupled and thus totally the singlet ground state is formed in $[Fe_4S_4]^{2+}$.

In the present paper, we study the electronic structures of $[Fe_2S_2(SCH_3)_4]^{2-,3-}$ in polar solvent. Although $Fe_2S_2$ clusters have been the subjects of many theoretical studies, most of them are based on spin-unrestricted Hartree−Fock (UHF) or density functional theory (DFT).[7,9,10,15] We employ here spin-adapted wave functions, that is, complete active space self-consistent field (CASSCF) and multireference second-order Møller−Plesset perturbation theory (MRMP),[16] to calculate the energy levels of all the spin states including the intermediate ones. The spin-adapted method is particularly important for describing the delocalized $Fe^{2.5+}Fe^{2.5+}$ reduced state because the spin-unrestricted method with symmetry-broken molecular orbitals is difficult to apply to this state. Solvent environmental effects on the electronic structures of the $[Fe_2S_2(SCH_3)_4]^{2-,3-}$ cluster are incorporated by the reference interaction site model (RISM) SCF method.[17] Mouesca et al.[7] and Li et al.[9] used a dielectric continuum model to evaluate the protein and solvent contributions to the redox potentials of iron−sulfur clusters. The advantage of the RISM-SCF method over the dielectric continuum model is that it maintains the molecular aspects of solvent and thus is capable of describing a local solute−solvent interaction in molecular detail.

The purposes of the present paper are twofold. One is to provide detailed descriptions of the electronic and magnetic properties of $[Fe_2S_2(SCH_3)_4]^{2-,3-}$ in polar solvent. Based on the calculated energies of various spin states, the spin interaction between two Fe ions is examined both for the oxidized and for the reduced forms, and the results are compared with the

10.1021/jp0581429 CCC: $30.25 
Published on Web 10/12/2005

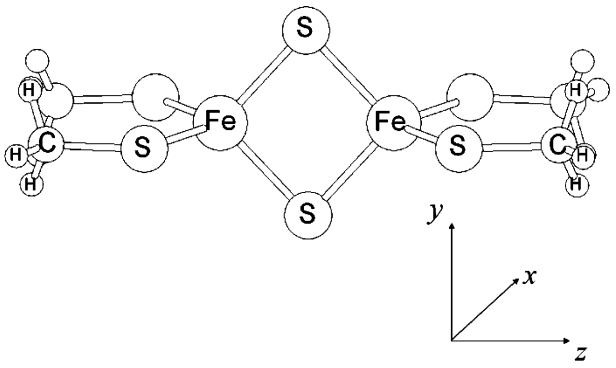


**Figure 1.** Strucure of $Fe_2S_2^*(SCH_3)_4$ cluster.

available experiments. For the reduced state, we focus on the relative stability between the localized and delocalized forms. It is noted that reliable electronic structure calculations for the delocalized $Fe^{2.5+}Fe^{2.5+}$ state are virtually nonexistent, to our knowledge. The other is to examine the effect of solvent thermal fluctuation on the activation barrier of the reduction process. We derive a simple model for calculating the free energy profiles based on the RISM-SCF method. In the next section, computational methods employed in the present work are described. In section 3, we present the calculated results. Electronic and magnetic properties of the oxidized and reduced states of the $Fe_2S_2$ cluster are discussed. We also examine the mechanism of the reduction process based on the calculated redox potentials and solvation structures. The conclusions are summarized in section 4.

## 2. Computational Details

We calculated the electronic structures of $[Fe_2S_2(SCH_3)_4]^{2-,3-}$ in polar solvent (see Figure 1). Although dimethyl formamide (DMF) has been used as a solvent in many experimental works, we adopt here dimethyl sulfoxide (DMSO) because DMSO with a smaller number of interaction sites is easier to treat than DMF and the experimental results in DMSO solution are not very different from those in DMF.[4,18]

In RISM-SCF theory, the free energy is given by

$$F = \langle \Psi | \hat{H}_0 | \Psi \rangle + \Delta\mu \tag{2}$$

where $\hat{H}_0$ is the solute electronic Hamiltonian in the gas phase, $\Psi$ is the solute wave function, and $\Delta\mu$ is the excess chemical potential.[17] If we employ the second-order perturbation theory to estimate the dynamic electron correlation energy, the free energy becomes

$$F = \langle \Psi | \hat{H}_0 | \Psi \rangle + \Delta E^{(2)} + \Delta\mu \tag{3}$$

Here $\Delta E^{(2)}$ is the second-order correlation energy calculated with the solvated Hamiltonian,

$$\hat{H} = \hat{H}_0 + \sum_a \hat{Q}_a V_a \tag{4}$$

where $\hat{Q}_a$ is the population operator generating the effective charge $Q_a$ at the solute site $a$ and $V_a$ is the electrostatic potential acting on the site $a$ obtained from RISM-SCF calculations. With this Hamiltonian, we can take account of the change of $\Delta\mu$ due to the first-order change of solute effective charges because this can be represented as

$$\Delta\mu(\mathbf{Q}^{(0)} + \Delta\mathbf{Q}^{(1)}) \approx \Delta\mu(\mathbf{Q}^{(0)}) + \sum_a \Delta Q_a^{(1)} V_a \tag{5}$$

and is included in eq 3. Here $\mathbf{Q}^{(0)}$ is the RISM-SCF effective charge on the solute sites and $\Delta\mathbf{Q}^{(1)}$ the first-order change of effective charges obtained from the first-order wave function.

CASSCF wave functions were constructed as follows. For the geometry optimizations of the oxidized and reduced states, we chose 10 active space orbitals that are mainly localized to the Fe 3d orbitals. To obtain more reliable energy estimates, the active space was increased to 13 by including three orbitals mainly composed of S* 3p atomic orbitals, $(p_y + p_y)$ with $b_{2u}$ symmetry, $(p_z + p_z)$ with $b_{1u}$, and $(p_z - p_z)$ with $b_{3g}$, to the active space. These CASSCF orbitals are displayed in Figure 2. For MRMP calculations, the intruder state avoidance method[19] with the parameter of 0.02 was applied. Note that change of the parameter little affected the calculated results.

The effective core potentials with the basis sets proposed by Stevens et al.[20,21] were employed for Fe and S. We further augmented diffuse s and p functions on S, and thus the resultant contracted basis functions were (8s8p6d)/[4s4p3d] and (5s5p1d)/[4s4p1d] for Fe and S, respectively. For C and H atoms, the 6-31G basis set was used. In determining the partial charges on the solute sites, grid points generated by the Spackman method[22] were applied.

The RISM integral equations were solved by using the hypernetted chain (HNC) closure relation. The Lennard-Jones (LJ) parameters and solvent partial charges are summarized in Table 1. Since the LJ parameters for Fe were not available, we constructed them so as to reproduce the MM3 van der Waals function[25] between Fe and O atoms. The temperature and density of DMSO solvent were 298.15 K and 0.008 49 molecules/Å$^3$, respectively.

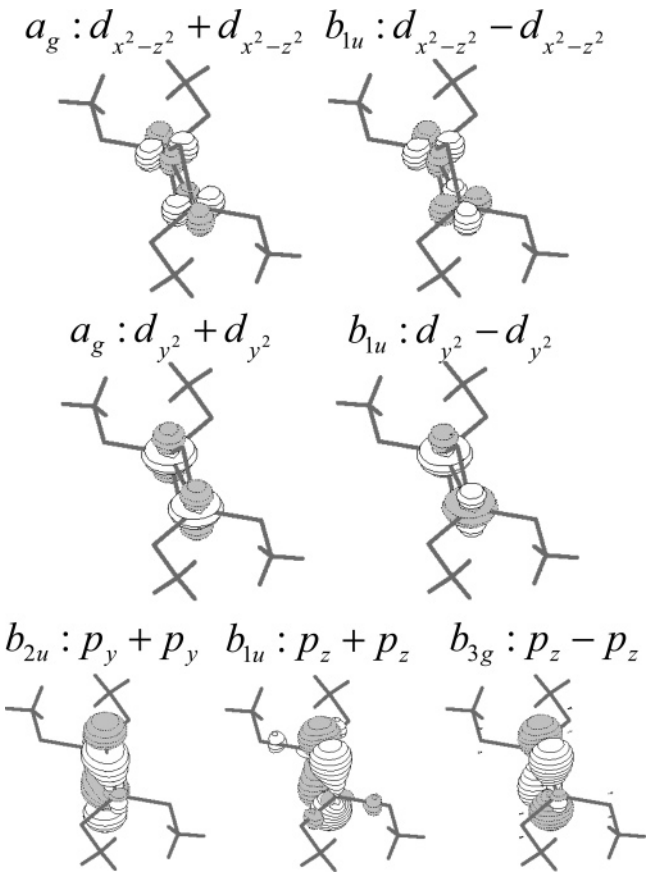


**Figure 2.** Important orbitals for describing the electronic structures: $d_{x^2-z^2} + d_{x^2-z^2}$ and $d_{x^2-z^2} - d_{x^2-z^2}$ orbitals (top), $d_{y^2} + d_{y^2}$ and $d_{y^2} - d_{y^2}$ orbitals (center), and three 3p orbitals on S* included in active space (bottom).

**TABLE 1: Lennard-Jones Parameters and Solvent Partial Charges**

| site | $q$ | $\sigma$, Å | $\epsilon$, kcal mol$^{-1}$ |
|---|---|---|---|
| | | Solute[a] | |
| Fe[b] | | 4.35 | 0.347 |
| S | | 3.56 | 0.250 |
| C | | 3.40 | 0.109 |
| H | | 2.47 | 0.016 |
| | | Solvent[c] | |
| O | −0.459 | 2.80 | 0.0715 |
| S | 0.139 | 3.40 | 0.238 |
| $CH_3$ | 0.160 | 3.80 | 0.293 |

[a] Reference 21. [b] See text for Fe parameters. [c] Reference 22.

**TABLE 2: CASSCF and MRMP-Optimized Geometries[a]**

| | | | reduced | | | |
|---|---|---|---|---|---|---|
| | oxidized | | localized | | delocalized | |
| | CASSCF | MRMP | CASSCF | MRMP | CASSCF | MRMP |
| Fe−S* | 2.356 | 2.207 | 2.326/2.525 | 2.214/2.321 | 2.413 | 2.223 |
| Fe−S | 2.416 | 2.312 | 2.475/2.561 | 2.360/2.408 | 2.540 | 2.385 |
| Fe−Fe | 3.167 | 2.697 | 3.224 | 2.855 | 3.046 | 2.619 |

[a] Units in Å.

All the calculations were performed by the GAMESS quantum chemistry package,[26] in which we implemented our own RISM-SCF routines.

## 3. Results and Discussion

**3.1. Electronic Structures.** *3.1.1. Oxidized State.* We examine here the electronic structure of the oxidized state, $[Fe_2S_2(SCH_3)_4]^{2-}$. For this state, the singlet spin state is observed experimentally as the ground state.[5,11,27] From structural points of view, two $Fe^{3+}$ ions are coordinated almost tetrahedrally by four $S^{2-}$ anions, which separates five Fe 3d orbitals into two groups; energetically lower $d_{y^2}$ and $d_{x^2-z^2}$ orbitals and higher $d_{xy}$, $d_{yz}$, and $d_{zx}$ ones, and these two $Fe^{3+}$ ions with $S = {}^5/_2$ spin multiplicity couple antiferromagnetically. Note that in the present case two lower orbitals split into $d_{y^2}$ and $d_{x^2-z^2}$ ones by a distortion from the regular tetrahedron (see Figure 2).

The optimized geometry at the RISM-CASSCF level is given in Table 2, where the calculated Fe−S* and Fe−S distances of 2.356 and 2.416 Å are much longer than the experimental ones, 2.185−2.232 and 2.303−2.312 Å.[4] This is because the CASSCF wave function mainly treats the static electron correlation effect, not the dynamic correlation. To obtain a more reliable estimate of the geometry, we carried out the RISM-CASSCF/MRMP calculations. Since the full geometry optimization with the MRMP method is computationally formidable for such a large system as $[Fe_2S_2(SCH_3)_4]^{2-}$ at present, we only optimized important distances with the method as follows. We first performed RISM-CASSCF calculations to optimize all the remaining degrees of freedom with fixing the Fe−S* and Fe−S distances, denoted as $r_i$ ($i$ = 1, ..., 8), at values around the CASSCF optimized geometry, and then calculated the RISM-CASSCF/MRMP free energies at these geometries. The resultant free energies were next represented by a quadratic function,

$$F(\mathbf{r}) = \frac{1}{2}\sum_{i,j} a_{ij} r_i r_j + \sum_i b_i r_i + c \qquad (6)$$

where the coefficients, $a_{ij}$, $b_i$, and $c$, were least-squares fitted to the energies at nine points: Fe−S* = 2.15, 2.20, and 2.25 Å and Fe−S = 2.25, 2.30, and 2.35 Å, respectively. The standard deviation between the calculated free energy and fitted function was $5.4 \times 10^{-5}$ hartree. Note that only two distances are independent variables because the oxidized form has $D_{2h}$ symmetry. The Fe−S* and Fe−S distances thus obtained are included in Table 2. Although these distances, 2.207 and 2.312 Å, are considerably improved from the CASSCF values, the Fe−Fe distance, 2.977 Å, is still longer than the experimental values, 2.691−2.698 Å. Therefore, we further carried out the RISM-CASSCF/MRMP calculations with varying the Fe−Fe distance, where the remaining bond distances were fixed. The resultant Fe−Fe distance, 2.697 Å, is now in good agreement with the experiments as seen in Table 2.[28]

**TABLE 3: Energies of Different Spin-States for the Oxidized States[a]**

| state | MRMP | | CASSCF | |
|---|---|---|---|---|
| $^{11}B_{1u}$ | 6093 | (6415) | 1583 | (1586) |
| $^{9}A_g$ | 4463 | (4713) | 1159 | (1161) |
| $^{7}B_{1u}$ | 2897 | (3066) | 750 | (751) |
| $^{5}A_g$ | 1539 | (1631) | 397 | (398) |
| $^{3}B_{1u}$ | 535 | (566) | 138 | (138) |
| $^{1}A_g$ | 0[b] | (0) | 0[b] | (0) |

[a] Values in parentheses are in a vacuum. Units are in cm$^{-1}$. [b] Relative energies with respect to $^1A_g$ states. MRMP and CASSCF energies of $^1A_g$ in solution are −465.1774 and −463.2827 hartree, respectively.

At the MRMP-optimized geometry, the energies of all the spin states, $S$ = 0−5, were calculated by the RISM-CASSCF and MRMP methods, and the relative energies with respect to the singlet state, $S$ = 0, are listed in Table 3. In experimental and theoretical studies for binuclear transition metal complexes, the Heisenberg Hamiltonian

$$H = -2J(\hat{\mathbf{S}}_1 \cdot \hat{\mathbf{S}}_2) \qquad (7)$$

has been conveniently utilized to model the spin interaction between different centers. Here $\hat{\mathbf{S}}_1$ and $\hat{\mathbf{S}}_2$ are the spin operators assigned to the two centers and the total spin $\mathbf{S}$ is given by $\hat{\mathbf{S}} = \hat{\mathbf{S}}_1 + \hat{\mathbf{S}}_2$. With this Hamiltonian, the energy of state with the spin quantum number $S$ is given by

$$E(S) = -JS(S+1) \qquad (8)$$

where $J$ is the spin−spin interaction parameter. As seen in Table 3, the calculated energy sequence significantly deviates from the prediction by the Heisenberg Hamiltonian. The energy difference between the nearest neighbor spin states becomes smaller with the increase of $S$ than that by eq 8, indicating that the parameter $|J|$ strongly depends on the quantum number $S$ and decreases with increasing $S$. Cory et al.[10] calculated the energy levels of all the spin states for $[Fe_2S_2SH_4]^{2-}$ by the projected UHF method with the semiempirical Zerner's intermediate neglect of differential overlap (ZINDO) Hamiltonian. In contrast to the present results, they observed that $|J|$ increased with increasing $S$. The present results can be rationalized by analyzing the wave functions. The occupation numbers of the 3d orbital pairs for the $S$ = 0 state are (1.009, 0.991), (1.148, 0.852), (1.046, 0.954), (1.123, 0.877), and (1.044, 0.956) for $d_{x^2-z^2}$, $d_{y^2}$, $d_{xy}$, $d_{yz}$, and $d_{zx}$, respectively. This means that the spin exchange interaction depends on the type of d orbital pair and the Heisenberg Hamiltonian is too simple to describe such complicated spin interactions as those in the present system. It is noteworthy that the occupation numbers gradually change with $S$ and become 1 at $S$ = 5, indicating that there is no particular UHF electronic configuration for the intermediate spin states.

As in the previous works,[7,9,10] we estimated the value of $J$ using the energies of $S$ = 5 and 0 states, and the results are

**TABLE 4: Energy Levels of the Reduced State in a Vacuum at the Oxidized State Geometry[a]**

| state | MC-QDPT | SA-CASSCF | |
|---|---|---|---|
| The Lowest Spin State ($S = {}^1/_2$) | | | |
| $^2B_{1u}$ | 0[b] | 0[b] | $d_{x^2-z^2} + d_{x^2-z^2}$ |
| $^2A_g$ | 0.050 | 0.050 | $d_{x^2-z^2} - d_{x^2-z^2}$ |
| $^2B_{1u}$ | 0.869 | 0.458 | $d_{y^2} + d_{y^2}$ |
| $^2A_g$ | 1.279 | 0.744 | $d_{y^2} - d_{y^2}$ |
| The Highest Spin State ($S = {}^9/_2$) | | | |
| $^{10}B_{1u}$ | 0.252 | 0.168 | $d_{y^2} + d_{y^2}$ |
| $^{10}A_g$ | 1.053 | 0.601 | $d_{x^2-z^2} - d_{x^2-z^2}$ |
| $^{10}B_{1u}$ | 1.135 | 0.636 | $d_{x^2-z^2} + d_{x^2-z^2}$ |
| $^{10}A_g$ | 3.193 | 1.954 | $d_{y^2} - d_{y^2}$ |

[a] Units in eV. [b] Relative energies with respect to $1^2B_{1u}$ states. MC-QDPT and SA-CASSCF energies of $1^2B_{1u}$ are $-465.0387$ and $-463.0490$ hartree, respectively.

$-53$ and $-203$ cm$^{-1}$ for the RISM-CASSCF and MRMP methods, respectively. The present MRMP value of $|J|$ is slightly larger than the results with the ZINDO Hamiltonian, 161 cm$^{-1}$, but is much smaller than the DFT result, 382 cm$^{-1}$. We also obtained the $|J|$ value from the energy difference between the $S = 1$ and 0 states, 268 cm$^{-1}$. Experimentally the value of $|J|$ has been measured for various ferredoxin complexes: 180 cm$^{-1}$ for spinach ferredoxin,[11] 182 cm$^{-1}$ for *Spirulina maxima*,[27] and 149 cm$^{-1}$ for a synthetic analogue.[5] The present results of $|J|$ are comparable to these experimental values.

As shown in Table 3, the energy differences between the nearest neighbor spin states by the CASSCF wave functions are much smaller that those by the MRMP. This is because the dynamic correlation energy becomes larger with decreasing $S$. The energy levels of all the spin states calculated in a vacuum at the same geometry as in solvent are also presented in the parentheses in Table 3, where we can see that the energy differences are insensitive to the solvent environment.

*3.1.2. Reduced State.* The electronic structure of the reduced state, $[Fe_2S_2(SCH_3)_4]^{3-}$, is more complicated than that of the oxidized one. There can be many electronic states when one electron is inserted into the oxidized state. As noted above, the $d_{y^2}$ and $d_{x^2-z^2}$ orbitals of Fe are energetically lower than the other three d orbitals in the oxidized state, and therefore one can expect that an electron is added to one of the four orbitals $d_{y^2} + d_{y^2}$, $d_{y^2} - d_{y^2}$, $d_{x^2-z^2} + d_{x^2-z^2}$, and $d_{x^2-z^2} - d_{x^2-z^2}$ in forming the ground state of the reduced one (see Figure 2). To specify the ground-state electronic structure, we first carried out four states averaged (SA) CASSCF calculations for the reduced states with the lowest and highest spin multiplicities, $S = {}^1/_2$ and ${}^9/_2$, at the MRMP-optimized geometry for the oxidized state. Here we employed 13 active orbitals, and 17 electrons were distributed among them. In this case, the dynamic electron correlation energies were estimated by the multiconfigurational quasi-degenerate perturbation theory (MC-QDPT).[29] Note that the MC-QDPT method becomes the same as the MRMP when only one state is considered.

Table 4 summarizes the calculated energies. For the low-spin state, $S = {}^1/_2$, the $^2B_{1u}$ state is energetically the lowest both from the SA-CASSCF and MC-QDPT calculations. As seen in the table, the second state, $^2A_g$, is located at very close in energy to the $^2B_{1u}$, though the energies of the third and fourth states are much higher than that of the ground state. If we employ the CASSCF wave functions with 10 active orbitals, the occupation number of the $d_{x^2-z^2} + d_{x^2-z^2}$ orbital is $\sim$2 with those of the remaining active orbitals being $\sim$1 for the ground state, while the $d_{x^2-z^2} - d_{x^2-z^2}$ orbital has the occupation of $\sim$2 in the $^2A_g$. However, the occupation numbers of these two $d_{x^2-z^2}$ orbitals becomes $\sim$1.5 if the number of active orbitals is increased to 13. This is because the wave function of $S = {}^1/_2$ state is described as a linear combination of electronic configurations corresponding to two localized structures, $Fe^{2+}Fe^{3+}$ and $Fe^{3+}$-$Fe^{2+}$, at $D_{2h}$ geometry and the mixing of S* orbitals with Fe 3d ones is allowed so as to stabilize the Fe ions by including the S* orbitals into the active space. We found that the CASSCF wave function is unstable with respect to the symmetry breaking of CASSCF orbitals[30] and that the CASSCF energy with 10 active orbitals is actually lowered by 2.1 eV by removing the restriction of $D_{2h}$ symmetry to the orbitals. Two $d_{x^2-z^2}$ CASSCF orbitals thus obtained were localized to different Fe atoms and the occupation numbers obtained from the symmetry-broken CASSCF wave function were $\sim$2 for one $d_{x^2-z^2}$ orbital and $\sim$1 for the other.

The high-spin ground state is $^{10}B_{1u}$ where the $d_{y^2} + d_{y^2}$ orbital with $a_g$ symmetry is doubly occupied and the remaining d orbitals are singly occupied. As shown in Table 4, the ground-state energy is well separated from those of the excited ones. The electronic structure of this state is characterized as a delocalized state, $Fe^{2.5+}Fe^{2.5+}$, where the electron inserted into the oxidized state distributes over two Fe atoms. For the delocalized state, the double exchange mechanism has been proposed to interpret the energy levels for states with different spin multiplicities,[31−33] where the double exchange parameter $B$ is added to the Heisenberg Hamiltonian, eq 7, and thus the energy levels are given by

$$E(S) = -JS(S+1) - B(S+{}^1/_2) \qquad (9)$$

where $B$ is defined to be positive. From eq 9, the highest spin state, $S = {}^9/_2$, can be the ground state for $|B/J| > {}^9/_2$ with $J < 0$. Based on the Hubbard−Anderson model Hamiltonian, Girerd et al.[33] showed that the magnitude of $B$ is proportional to the interaction energy between the two d orbitals that the delocalized electron occupies, and such an interaction energy is roughly estimated as a half of the energy gap between the bonding and antibonding orbitals formed by a pair of d orbitals. We estimated the energy gaps using the CASSCF canonical orbitals for the oxidized state, and the results were 1.11, 2.76, 1.01, 0.30, and 3.55 eV for the $d_{xy}$, $d_{yz}$, $d_{zx}$, $d_{x^2-z^2}$, and $d_{y^2}$ orbital pairs, respectively. Considering that the gap between the $d_{x^2-z^2} \pm d_{x^2-z^2}$ orbitals is the smallest and that between the $d_{y^2} \pm d_{y^2}$ orbitals is the largest among the five d orbital pairs, the results in Table 4 are consistent with the prediction derived from the double exchange mechanism.

We carried out geometry optimizations for the reduced state in DMSO solvent with the same procedures as those for the oxidized state. For the low-spin state, we employed the CASSCF method with 10 symmetry-broken active orbitals even at a $D_{2h}$ geometry. The resultant optimized geometries are summarized in Table 2. As in the case of oxidized state, the Fe−S* and Fe−S distances at the MRMP-optimized geometries become shorter by 0.1−0.2 Å than those of the CASSCF geometries both for the localized and for the delocalized states. The low-spin localized state with $S = {}^1/_2$ has the $C_{2v}$ optimized geometry, where the Fe−S* and Fe−S distances at $Fe^{2+}$ side are lengthened by 0.1 Å from the oxidized state. The $D_{2h}$-optimized geometry was obtained for the high-spin delocalized state, $S = {}^9/_2$. Both the Fe−S* and Fe−S bond lengths become slightly longer than those in the oxidized state. It is noted that the Fe−Fe distance shrinks from that in the oxidized state because the $d_{y^2} + d_{y^2}$ bonding orbital becomes doubly occupied in the delocalized high-spin state.

**TABLE 5: Energies of Different Spin-States for the Reduced States[a]**

| localized | | | delocalized | | |
|---|---|---|---|---|---|
| state | MRMP | CASSCF | state | MRMP | CASSCF |
| $^{10}A_1$ | 2514 (2802) | 851 (846) | $^{10}B_{1u}$ | −2707 (−2346) | −4298 (−4286) |
| $^{8}A_1$ | 1944 (2119) | 578 (575) | $^{8}A_g$ | −2285 (−1999) | −3275 (−3263) |
| $^{6}A_1$ | 1129 (1246) | 328 (327) | $^{6}B_{1u}$ | −1839 (−1606) | −2219 (−2209) |
| $^{4}A_1$ | 453 (504) | 129 (128) | $^{4}A_g$ | −1087 (−930) | −1117 (−1110) |
| $^{2}A_1$ | 0 (0)[b] | 0 (0)[b] | $^{2}B_{1u}$ | 0 (0)[b] | 0 (0)[b] |

[a] Values in parentheses are in a vacuum. Units are in $cm^{-1}$. [b] Relative energies with respect to $^2A_1$ for the localized states and $^2B_{1u}$ for the delocalized ones, respectively. MRMP and CASSCF energies of the $^2A_1$ states in solution are −464.9759 and −463.1129 hartree, respectively. Those of the $^2B_{1u}$ states are −464.9962 and −463.0179 hartree, respectively.

To examine the spin interaction in the reduced state, we calculated the energies of states with all the possible spin multiplicities at the MRMP-optimized geometries for the localized and delocalized states. The electrostatic potentials acting on the solute atomic sites were obtained by the RISM-CASSCF calculations for each state. The results are summarized in Table 5. For the localized state, the ground state is $^2A_1$, and the energy becomes higher with increasing $S$, though the level structure largely deviates from that of eq 8 as seen in the oxidized state. The spin interaction parameter $|J|$ estimated from the energies of $S = {}^9/_2$ and ${}^1/_2$ states is 105 $cm^{-1}$, which agrees with the experimental values, $\leq$100 $cm^{-1}$ for spinach ferredoxin[11] and 98 $cm^{-1}$ for *Spirulina maxima*.[27] In contrast to the localized state, the highest spin state, $S = {}^9/_2$, is the lowest in energy for the delocalized state, and the energy becomes high with decreasing $S$. We obtained the values of $J$ and $B$ by least-squares fitting to the energy levels in Table 5, and the results were −115 and 1367 $cm^{-1}$ for $J$ and $B$, respectively. The calculated double exchange $B$ term is very close to the experimental value, 1430 $cm^{-1}$, estimated from variable temperature magnetic circular dichroism (MCD) spectra of the reduced Cys60Ser mutant of *Clostridium pasteurianum* 2Fe ferredoxin.[13]

The high-spin delocalized state has been suggested to exist in protein mutants, and its ratio to the amount of localized state has been estimated to be 1.5 from the MCD magnetization data of the Cys60Ser mutant of *Clostridium pasteurianum*[13] and 0.4 from the Mössbauer spectra of the Cys56Ser mutant.[14] We estimated the relative stability between the localized and delocalized states from the present calculations. The delocalized state is calculated to be more stable than the localized one by 0.58 eV by the RISM-CASSCF/MRMP calculations with 10 active orbitals. However, the 10 active space is not sufficient for describing the localized state, as mentioned above, and therefore we further carried out four SA-CASSCF and MC-QDPT calculations with 13 active orbitals for both the states to obtained a more reliable estimate of the energy difference. As seen in Table 6, the localized state becomes lower in energy by 0.09 eV than the delocalized one. Although the relative stability between the two electronic states depends on the level of calculations and is difficult to estimate accurately, we can at least conclude that the delocalized state lies close in energy to the localized one.

**3.2. Redox Process.** The redox potential $E^0$ is defined by

$$E^0 = \Delta F_{red} + \Delta(\mathrm{SHE}) \tag{10}$$

where $\Delta F_{red}$ is the difference of free energies between the reduced and oxidized states and $\Delta$(SHE) is the standard hydrogen electrode potential. The free energy difference is further decomposed as

$$\Delta F_{red} = \mathrm{IP}_{red} + \Delta F_{solv} \tag{11}$$

Here $IP_{red}$ is the ionization potential of the reduced state in the gas phase and $\Delta F_{solv}$ is the change of solvation free energy due to the reduction of the oxidized state. We performed the RISM-CASSCF/MRMP calculations with 13 active orbitals for the oxidized state to be consistent with the reduced state energies with 13 active orbitals. Table 6 summarizes the calculated free energy differences and their components.

**TABLE 6: Differences of Free Energies between the Reduced and Oxidized States[a]**

| state | | $\Delta F_{red}$ | $IP_{red}$ | $\Delta F_{solv}$ |
|---|---|---|---|---|
| MRMP (10 Active Orbitals)[b] | | | | |
| vertical | localized | 1.708 (−0.960) | −5.498 (−7.964) | 7.206 (7.004) |
| | delocalized | 2.359 (−0.183) | −4.896 (−7.239) | 7.255 (7.056) |
| adiabatic | localized[c] | 1.894 (−0.274) | −5.158 (−6.540) | 7.052 (6.266) |
| | delocalized | 2.472 (0.389) | −4.612 (−6.513) | 7.084 (6.902) |
| MC-QDPT (13 Active Orbitals)[d] | | | | |
| vertical | localized | 2.766 (0.257) | −4.399 (−6.740) | 7.165 (6.997) |
| | delocalized | 2.717 (0.239) | −4.652 (−6.908) | 7.369 (7.147) |
| adiabatic | localized | 2.870 (1.553) | −4.215 (−5.395) | 7.085 (6.948) |
| | delocalized | 2.782 (0.763) | −4.412 (−6.221) | 7.194 (6.984) |

[a] Values in parentheses are obtained by RISM-CASSCF calculations. Units are in eV. [b] RISM-CASSCF/MRMP free energy of the oxidized state is −465.3915 hartree with 10 active orbitals. [c] We obtained the free energy by adding the difference between the vertical and adiabatic free energies by broken-symmetry calculations to the vertical free energy calculated with $D_{2h}$ symmetry kept. [d] RISM-CASSCF/MRMP free energy of the oxidized state is −465.4024 hartree with 13 active orbitals.

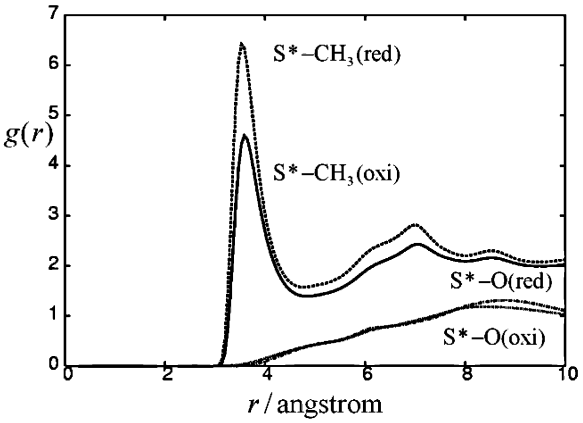


**Figure 3.** Radial distribution functions between S* and solvent sites: oxidized state, $CH_3$ (solid line) and O (dotted line); reduced state, $CH_3$ (dashed line) and O (dot−dashed line).

The gas-phase vertical ionization potentials were calculated to be −4.4 and −4.7 eV for the low-spin localized and high-spin delocalized reduced states, respectively, at the MC-QDPT level. The dynamic electron correlation effect reduces the magnitudes of $IP_{red}$ more than 2 eV from the CASSCF values. The adiabatic ionization energies obtained at the MRMP-optimized geometries for the reduced forms become −4.2 and −4.4 eV, respectively. Although the energies of the reduced states are higher than that of the oxidized one in the gas phase, the solvation energies increase by redistributing the solvent so as to be in equilibrium to the reduced state charges. Figure 3 shows the radial distribution functions between the bridging S* atom and the solvent sites, where we can see that the S*−$CH_3$ peak grows by forming the reduced state, while the S*−O

distribution shows small change. As seen in Table 6, the free energy differences, $\Delta F_{red}$, become 2.77 and 2.72 eV at the geometry of the oxidized state and further increase to 2.87 and 2.78 eV at the equilibrium geometries of the localized and delocalized states, respectively, at the MC-QDPT level, while the CASSCF redox potentials are considerably small. Experimentally, the free energy difference between the oxidized and reduced states was estimated to be 3.18 eV for $[Fe_2S_2(S_2\text{-}o\text{-xylyl})_2]^{2-}$ and 3.58 eV for $[Fe_2S_2(SPh)_4]^{2-}$.[4] Note that larger redox potentials may be obtained if we replace the $CH_3$ group by *o*-xylyl or phenyl one because the gas-phase reduced state energy can be lowered by distributing the added electron over these aromatic rings.

We now consider the activation barrier of the reduction reaction. Since the low-spin localized state is directly formed by adding an electron to the oxidized state, we adopt here the localized state as the reduced state. In describing charge-transfer reactions in solution, it is convenient to employ the potential energy difference between the two states as a solvation coordinate, *s*.[34−37] Since the solute−solvent interaction is represented by the site−site electrostatic and LJ potentials in the RISM-SCF theory, the solvation coordinate *s* is calculated as the function of electrostatic potentials **V** acting on the solute sites with the Hamiltonian eq 4,

$$s = E^{red}(\mathbf{V};\mathbf{R}) - E^{oxi}(\mathbf{V};\mathbf{R}) \tag{12}$$

where $E^{red}$ and $E^{oxi}$ are the energies of reduced and oxidized states, respectively, at the solute nuclear coordinate **R**. Note that the LJ energy does not contribute to *s* because we employ the same LJ parameters both for the oxidized and reduced states.

The free energy surface of the oxidized state can be defined by

$$F^{oxi}(s,\mathbf{R}) = -\beta^{-1} \ln P(s;\mathbf{R}) + C(\mathbf{R}) \tag{13}$$

where $P(s;\mathbf{R})$ is the probability density of *s* and $\beta^{-1} = k_B T$ with $k_B$ the Boltzmann constant and *T* the temperature, respectively. Here $C(\mathbf{R})$ is independent of *s* and is determined later. The probability $P(s;\mathbf{R})$ is given by

$$P(s;\mathbf{R}) = \int \delta\{s - E^{red}(\mathbf{V};\mathbf{R}) + E^{oxi}(\mathbf{V};\mathbf{R})\} W(\mathbf{V};\mathbf{R})\, d\mathbf{V} \tag{14}$$

where $W(\mathbf{V};\mathbf{R})$ is the probability function of the electrostatic potentials **V** acting on the solute sites for the oxidized state. We assume that *W* is represented by a multivariate Gaussian distribution function,

$$W(\mathbf{V};\mathbf{R}) = \left(\frac{1}{2\pi}\right)^{N/2} (\det \sigma(\mathbf{R})^{-1})^{1/2} \exp\left(-\frac{1}{2}\Delta\mathbf{V}^t \sigma(\mathbf{R})^{-1} \Delta\mathbf{V}\right) \tag{15}$$

where $\Delta\mathbf{V}$ is the deviation of the electrostatic potentials from the average values obtained from the equilibrium solvation in the oxidized state, $\Delta\mathbf{V} = \mathbf{V} - \bar{\mathbf{V}}$. The matrix element $\sigma_{ab}$ of $\sigma$ represents the correlation between the fluctuations of electrostatic potentials at the solute sites *a* and *b*,

$$\sigma_{ab} = \langle \Delta V_a \Delta V_b \rangle \tag{16}$$

which can be analytically calculated with the RISM equations.[38]

We also assume that the electronic energies are expanded to the first order in $\Delta\mathbf{V}$,

$$E^K(\mathbf{V}) = E^K(\bar{\mathbf{V}}) + \sum_a^N \left(\frac{\partial E^K}{\partial V_a}\right)_{\bar{V}} \Delta V_a$$

$$= E^K(\bar{\mathbf{V}}) + \sum_a^N Q_a^K \Delta V_a \quad (K = \text{oxi or red}) \tag{17}$$

where $Q_a^K$ is the effective charge at the site *a* in the oxidized or reduced state. To calculate the probability *P*, it is convenient to diagonalize the covariance matrix $\sigma$,

$${}^tU\sigma U = \Lambda \tag{18}$$

where $\Lambda$ is the diagonal matirx with the elements $\Lambda_i$ ($i = 1, 2, ..., N$). From eqs 14−18, the probability function can be analytically calculated to be

$$P(s) = \left(\sum_{i=1}^N 2\pi\Lambda_i \Delta Q_i^2\right)^{-1/2} \exp\left[-\left(\sum_i^N 2\Lambda_i \Delta Q_i^2\right)^{-1} (s - s_{min})^2\right] \tag{19}$$

where

$$\Delta Q_i = \sum_a^N (Q_a^{red} - Q_a^{oxi}) U_{ai} \tag{20}$$

and

$$s_{min} = E^{red}(\bar{\mathbf{V}}) - E^{oxi}(\bar{\mathbf{V}}) \tag{21}$$

where $U_{ai}$ represents the eigenvector of $\sigma$. The oxidized state free energy is thus expressed as

$$F^{oxi}(s;\mathbf{R}) = \frac{1}{2} k(\mathbf{R})(s - s_{min}(\mathbf{R}))^2 + F_0^{oxi}(\mathbf{R}) \tag{22}$$

where $C(\mathbf{R})$ in eq 13 is chosen so that the value of $F^{oxi}(s;\mathbf{R})$ becomes that for the equilibrium solvation $F_0^{oxi}$ at $s = s_{min}$ and the force constant *k* is given by

$$k = \frac{1}{\beta \sum_i \Lambda_i \Delta Q_i^2} \tag{23}$$

The parabolic free energy curve for the reduced state is obtained using the relation[35−37]

$$F^{red}(s;\mathbf{R}) - F^{oxi}(s;\mathbf{R}) = s \tag{24}$$

and the activation energy for the reduction process is calculated by

$$\Delta F^{\ddagger}(\mathbf{R}) = \frac{s_{min}(\mathbf{R})^2}{4\lambda(\mathbf{R})} \tag{25}$$

where $\lambda = 1/(2k)$ is the reorganization energy.

Figure 4 shows the calculated free energy curves for the oxidized and localized reduced states at the equilibrium geometry of the oxidized state, where the crossing of free energy curves is observed in the inverted region. The activation barrier height is calculated to be 0.32 eV (7.4 kcal/mol), indicating that the activation energy is low enough for an efficient reduction reaction to occur for the present system. Note that the reorganization energy was calculated to be 1.31 eV. We also calculated the barrier height at the equilibrium geometry of the localized reduce state, and the result was 14.6 kcal/mol,

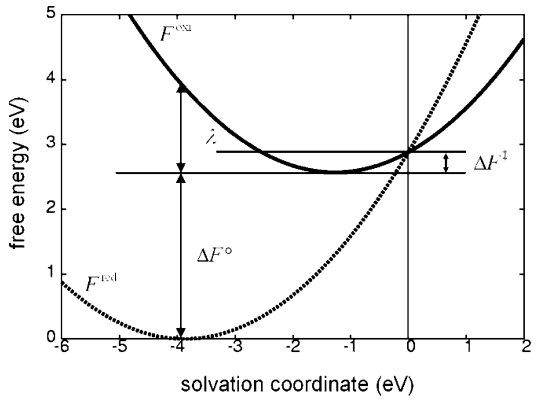


**Figure 4.** Calculated free energy curves for the reduction process.

which suggests that the reduction occurs near the equilibrium geometry of the oxidized state, that is, the vertical transition.

To access the reliability of the present simple free energy model, we estimated the free energy difference between the oxidized and reduced states. By comparison with the Marcus relation[39] for the activation energy,

$$\Delta F^{\ddagger} = \frac{(\lambda - \Delta F^\circ)^2}{4\lambda} \tag{26}$$

the free energy difference, that is, the reaction free energy, is given by

$$\Delta F^\circ = \lambda - s_{\min} \tag{27}$$

which is calculated to be −2.61 eV, comparable to the free energy difference in Table 6, −2.77 eV. This means that the present model can provide a good approximation of the free energy profiles for the reduction process despite rather crude assumptions, eqs 15 and 17, based on the linear response theory.

With the present model, we can analyze the importance of solvent fluctuation effect on the reduction reaction. As seen in eq 23, the reorganization energy is represented by the sum of the contributions from solvent polarization modes, $\Lambda_i \Delta Q_i^2$. In Figure 5, we show three polarization modes of which the contributions to $\lambda$ are more than 1%, $\Lambda_1$, $\Lambda_5$, and $\Lambda_{20}$, where the indices are the eigenvector numbers of $\sigma$ aligned with the decreasing order of the eigenvalues. The polarization mode with the largest eigenvalue was found to contribute over 92%, and the remaining 23 modes have small contributions. It is noteworthy that the polarization modes with small amplitudes on the $Fe_2S_2$ site do not contribute to $\lambda$ even if their eigenvalues are large. As discussed above, the $CH_3$ site of the DMSO solvent is already attracted by the negative charge of solute cluster in the initial oxidized state where the electrostatic potentials on the solute sites have positive values, 4.2−6.2 V. After forming the reduced state, these potentials become larger by 2.3−2.8 V, which indicates that the solute−solvent attractive interaction is enhanced. Therefore, the solvent mode responsible for the reduction process is considered to be approaching motions of the solvent molecules to the solute. The eigenvector corresponding to the most important polarization mode has the same sign of amplitude at all the solute sites as seen in Figure 5.

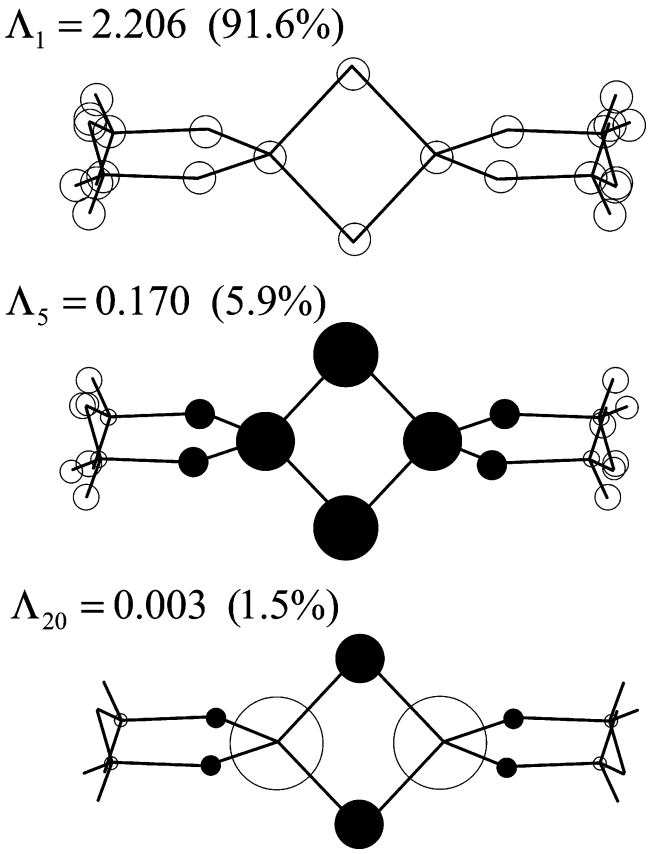


**Figure 5.** Important polarization modes. Λ is the eigenvalue ($10^{-3}$ au), and the value in parentheses is the contribution to the reorganization energy. The radius of the circle at each site is proportional to the site amplitude of the eigenvector with the white or black circle being the positive or negative sign.

## 4. Conclusion

In the present paper, we carried out RISM-CASSCF/MRMP calculations to study the electronic and magnetic properties of $[Fe_2S_2(SCH_3)_4]^{2-,3-}$ in DMSO solvent. For the reduced state, we found two states that were close in energy. One is the low-spin ($S = {}^1/_2$) localized state with $C_{2v}$ geometry, and the other is the high-spin ($S = {}^9/_2$) delocalized one with $D_{2h}$. This result is consistent with the experimental observations for mutants of *Clostridium pasteurianum*. The spin interaction parameters were estimated from the calculated energy levels of states with various spin multiplicities. The calculated spin−spin interaction parameters $J$ in the Heisenberg Hamiltonian were comparable to the available experimental estimates. The double exchange $B$ term was also obtained for the delocalized reduced state. It is noted here that we employed the 6-31G basis set for the $CH_3$ group. We repeated the energy calculations with the 6-31G* basis set using the same geometries as the 6-31G case. The energy gaps between spin states calculated with the 6-31G* basis set deferred only by about 5 $cm^{-1}$ from the 6-31G results, indicating that the $CH_3$ group can be regarded as a spectator to the electronic structures of the $Fe_2S_4$ cluster. The 6-31G* solute−solvent interaction energies were almost the same as those with the 6-31G basis set.

The redox potentials were estimated from the present calculations, 2.87 and 2.78 eV for the localized and delocalized reduced states, respectively. We also devised a simple model for the free energy profiles of the redox process based on the RISM-SCF theory. The transition state was located in the inverted region, and the barrier height was estimated to be 7.4 kcal/mol at the equilibrium geometry of oxidized state, indicating that the reduction reaction easily occurs for the present system. The solvent polarization modes important in determining the reorganization energy were analyzed. It was also found that the linear response assumption employed in constructing the present free energy model provides a good approximation for describing the redox process.

As seen in the present paper, the effect of solvent environment and its fluctuation is crucial in describing the redox processes of $Fe_2S_2$ clusters. This will be also true for iron−sulfur proteins where the fluctuation of protein and solvent environments plays an important role. In this respect, the results of the present calculations may provide valuable information for constructing realistic models of iron−sulfur protein systems for studying their biological functions.

**Acknowledgment.** This work was supported by the Grant-in-Aid from the Ministry of Education and Science, Japan.

## References and Notes

(1) Cammack, R. *Adv. Inorg. Chem.* **1992**, *38*, 281.

(2) Beinert, H.; Holm, R. H.; Münck, E. *Science* **1997**, *277*, 653 and references therein.

(3) Tsibris, J. C. M.; Woody, R. W. *Coord. Chem. Rev.* **1970**, *5*, 417.

(4) Mayerle, J. J.; Denmark, S. E.; DePamphilis, B. V.; Ibers, J. A.; Holm, R. H. *J. Am. Chem. Soc.* **1975**, *97*, 1032.

(5) Gillum, W. O.; Frankel, R. B.; Foner, S.; Holm, R. H. *Inorg. Chem.* **1976**, *15*, 1095.

(6) Noodlemen, L.; Peng, C. Y.; Case, D. A.; Mouesca, J.-M. *Coord. Chem. Rev.* **1995**, *144*, 199.

(7) Mouesca, J.; Chen, J. L.; Noodleman, L.; Bashford, D.; Case, D. A. *J. Am. Chem. Soc.* **1994**, *116*, 11898.

(8) Stephens, P. J.; Jollie, D. R.; Warshel, A. *Chem. Rev.* **1996**, *96*, 2491.

(9) Li, J.; Nelson, M. R.; Peng, C. Y.; Bashford, D.; Noodleman, L. *J. Phys. Chem. A* **1998**, *102*, 6311.

(10) Cory, M.; Stavrev, K.; Zerner, M. C. *Int. J. Quantum Chem.* **1997**, *63*, 781.

(11) Palmer, G.; Dunham, W. R.; Fee, J. A.; Sands, R. H.; Iizuka, T.; Yonetani, T. *Biochim. Biophys. Acta* **1971**, *245*, 201.

(12) Münck, E.; Debrunner, P. G.; Tsibris, J. C. M.; Gunsalus, I. C. *Biochemisty* **1972**, *11*, 855.

(13) Crouse, B. R.; Meyer, J.; Johnson, M. K. *J. Am. Chem. Soc.* **1995**, *117*, 9612.

(14) Achim, C.; Golinelli, M.; Bominaar, E. L.; Meyer, J.; Münck, E. *J. Am. Chem. Soc.* **1996**, *118*, 8168.

(15) O'Brien, T. A.; Davidson, E. R. *Int. J. Quantum Chem.* **2003**, *92*, 294.

(16) Hirao, K. *Chem. Phys. Lett.* **1992**, *190*, 374; *Chem. Phys. Lett.* **1992**, *196*, 397; *Chem. Phys. Lett.* **1993**, *201*, 59.

(17) Ten-no, S.; Hirata, F.; Kato, S. *Chem. Phys. Lett.* **1993**, *214*, 391; *J. Chem. Phys.* **1994**, *100*, 7453. Sato, H.; Hirata, F.; Kato, S. *J. Chem. Phys.* **1996**, *105*, 1546.

(18) DePamphilis, B. V.; Averill, B. A.; Herskovitz, T.; Que, L., Jr.; Holm, R. H. *J. Am. Chem. Soc.* **1974**, *96*, 4159.

(19) Witek, H. A.; Choe, Y.; Finley, J. P.; Hirao, K. *J. Comput. Chem.* **2002**, *23*, 957.

(20) Stevens, W. J.; Basch, H.; Krauss, M. *J. Chem. Phys.* **1984**, *81*, 6026.

(21) Stevens, W. J.; Krauss, M.; Basch, H.; Jasien, P. G. *Can. J. Chem.* **1992**, *70*, 612.

(22) Spackman, M. A. *J. Comput. Chem.* **1996**, *17*, 1.

(23) Cornell, W. D.; Cieplak, P.; Bayly, C. I.; Gould, I. R.; Merz, K. M., Jr.; Ferguson, D. M.; Spellmeyer, D. C.; Fox, T.; Caldwell, J. W.; Kollman, P. A. *J. Am. Chem. Soc.* **1995**, *117*, 5179.

(24) Luzar, A.; Soper, A. K.; Chandler, D. *J. Chem. Phys.* **1993**, *99*, 6836.

(25) Allinger, N. L.; Zhou, X.; Bergsma, J. *J. Mol. Struct. (THEOCHEM)* **1994**, *312*, 69.

(26) Schmidt, M. W.; Baldridge, K. K.; Boatz, J. A.; Elbert, S. T.; Gordon, M. S.; Jensen, J. J.; Koseki, S.; Matsunaga, N.; Nguyen, K. A.; Su, S.; Windus, T. L.; Dupuis, M.; Montgomery, J. A. *J. Comput. Chem.* **1993**, *14*, 1347.

(27) Petersson, L.; Cammack, R.; Rao, K. K. *Biochim. Biophys. Acta* **1980**, *622*, 18.

(28) For comparison with the CASSCF and MRMP geometries, we also performed the RISM-DFT(B3LYP) geometry optimization. The resultant distances are 2.290, 2.375, and 2.993 Å for Fe−S*, Fe−S, and Fe−Fe, respectively.

(29) Nakano, H. *J. Chem. Phys.* **1993**, *99*, 7983.

(30) For symmetry breaking of CASSCF wave functions, see, for example: Eisfeld, W.; Morokuma, K. *J. Chem. Phys.* **2000**, *113*, 5587.

(31) Zener, C. *Phys. Rev.* **1951**, *82*, 403. Anderson, P. W.; Hasegawa, H. *Phys. Rev.* **1955**, *100*, 675.

(32) Blondin, G.; Girerd, J.-J. *Chem. Rev.* **1990**, *90*, 1359.

(33) Girerd, J.-J.; Papaefthymiou, V.; Surerus, K. K.; Münck, E. *Pure Appl. Chem.* **1989**, *61*, 805.

(34) Hwang, J. K.; Warshel, A. *J. Am. Chem. Soc.* **1987**, *109*, 715.

(35) Tachiya, M. *Chem. Phys. Lett.* **1989**, *159*, 505.

(36) Kato, S.; Amatatsu, Y. *J. Chem. Phys.* **1990**, *92*, 7241.

(37) Ando, K.; Kato, S. *J. Chem. Phys.* **1991**, *95*, 5966.

(38) Naka, K.; Morita, A.; Kato, S. *J. Chem. Phys.* **1999**, *110*, 3484.

(39) Marcus, R. A. *J. Chem. Phys.* **1956**, *24*, 966; *J. Chem. Phys.* **1956**, *24*, 979.